Kinetic Lability, Structural Diversity, and Oxidation Reactions of New Oligomeric, Anionic Carboxylate−Pyridine Complexes

R. A. Reynolds III, W. R. Dunham, and D. Coucouvanis*

Department of Chemistry, The University of Michigan, Ann Arbor, Michigan 48109-1055

Received December 8, 1997

The dimeric $[M_2(OAc)_5(py)_2\mu\text{-}(OH_2)]Et_4N$ complexes, **I** (M = Mn, Fe, Co), have been isolated from pyridine solutions of $M^{II}(OAc)_2{\cdot}xH_2O$ and $Et_4N(OAc){\cdot}4H_2O$. The X-ray structures of **I** (M = Mn, Fe, Co) have been determined and show the metal ions asymmetrically bridged by two acetate ligands and a water molecule. One of the metal ions is bound by a pyridine ligand and two monodentate acetate ligands that are hydrogen bonded to the bridging water molecule. The second metal ion is bound to a bidentate acetate ligand and a pyridine ligand. Recrystallization of **I** from acetonitrile leads to the reorganization of **I** and isolation of the $M_3(OAc)_8(Et_4N)_2$ complexes, **II** (M = Mn, Fe, Co). The X-ray structure of **II** (M = Mn, Co) has been determined and shows the three metal ions connected by four bridging acetate ligands in a μ_1, μ_2 mode and two acetate ligands in the μ_1,η_1 mode, with a bidentate acetate ligand on each of the external metal ions completing the distorted octahedral geometry. Air oxidation of **I-Fe** in propionitrile leads to the formation of the mixed-valence $[Fe_3\mu_3\text{-}(O)(OAc)_7(OH_2)]Et_4N$ **(III)**. The X-ray structure of **III** has been determined and resembles the core of the basic acetate complexes; however, it has five bridging acetate ligands. The Mössbauer spectrum of **III** shows two quadrupole doublets in a 1:2 ratio with $\delta(Fe) = 1.29(1)$ and 0.48 mm/s; $\Delta E_q = 1.89$ and 0.71 mm/s. The oxidation of **I-Fe** by H_2O_2/O_2 in pyridine solution in the presence of Cl^- ligands affords $Fe_4\mu_3\text{-}(O)_2(OAc)_6(py)_4Cl_2$ (**IV**). The X-ray structure of **IV** shows a rhombic $\{Fe^{III}_4(\mu_3\text{-}O)_2\}$ core previously found in iron and manganese chemistry. The reaction of ferrocenium ion with **I-Fe** under basic conditions in dichloromethane solution led to the formation of the familiar mixed-valence $Fe_3\mu_3\text{-}(O)(OAc)_6(py)_3$ complex (**V**) with the basic acetate structure. Complexes **I-Fe**, **II-Fe**, **III**, and **IV** catalyze the reaction of O_2 with adamantane under GiF conditions to give adamantanols and adamantanone. The similarity of the results in comparison to similar studies previously reported for iron/carboxylate complexes are noted and discussed.

Introduction

The activation of dioxygen and the oxygenation of various substrates in biology are processes often facilitated or catalyzed by dinuclear iron sites.[1] Outstanding examples of metalloenzymes that contain such sites are the methane monooxygenases, (MMO)[2] and ribonucleotide reductase (RRB2).[3] The involvement of a similar site in oxygen transport is known to be essential in the function of the hemerythrins (Hr).[4] The structures of MMO (both oxidized[5] and reduced[6] forms), RRB2,[7] and Hr[8] have been determined and show dinuclear iron sites that contain bridging carboxylates (glutamate, aspartate); oxo, hydroxo, or aqua ligands; and terminally coordinated, oxygen donors (carboxylates, H_2O) or nitrogen donor (histidine) ligands (Figure 1).

Dinuclear Mn sites also play important roles in biology.[9] They are present in the pseudocatalases from *Lactobacillus plantarum*[10] and *Thermus thermophilus*[11] as well as in certain ribonucleotide reductases (RR),[12] where they catalyze the disproportionation of H_2O_2 and the reduction of ribonucleotides, respectively.

Dimeric units with structural features similar to those found in the diiron and dimanganese enzymes are also present as components of trinuclear sites in certain zinc and manganese

(1) (a) Murray, K. S. *Coord. Chem. Rev.* **1974**, *12*, 1. (b) Lippard, S. J. *Angew. Chem., Int. Ed. Engl.* **1988**, *27*, 344−361. (c) Que, L., Jr.; Scarrow, R. C. In *Metal Clusters in Proteins*; Que, L., Jr., Ed.; American Chemical Society: Washington, DC, 1988; p 302. (d) Que, L., Jr.; True, A. E. *Progr. Inorg. Chem.* **1990**, *38*, 97−199. (e) Sanders-Loehr, J. In *Iron Protein Carriers and Iron Proteins*; Loehr, T. M., Ed.; VCH: New York, 1989; p 375−466. (f) Lynch, J. B.; Juarez-Garcia, C.; Que, L., Jr. *Biol. Chem.* **1989**, *264*, 8091−8096.

(2) (a)Woodland, M. P.; Patil, D. S.; Cammick, R.; Dalton, H. *Biochim. Biophys. Acta* **1986**, *873*, 237−242. (b) Fox, B. G.; Surerus, K. K.; Münck, E.; Lipscomb, J. D. *Biol. Chem.* **1988**, *263*, 10553−10556.

(3) (a) Sjöberg, B.-M.; Gräslund, A. *Adv. Inorg. Biochem.* **1983**, *5*, 87−110. (b) Lammers, M.; Follman, H. *Struct. Bonding* **1983**, *54*, 27−91.

(4) (a) Wilkins, R. G.; Harrington, P. C. *Adv. Inorg. Biochem.* **1983**, *5*, 51−85. (b) Wilkins, P. C.; Wilkins, R. G. *Coord. Chem. Rev.* **1987**, *79*, 195−214.

(5) Rosenzweig, A. C.; Frederick, C. A.; Lippard, S. J.; Nordlund, P. *Nature* **1993**, *366*, 537−543.

(6) Rosenzweig, A. C.; Nordlund, P.; Takahara, P. M.; Frederick, C. A.; Lippard, S. J. *Chem. Biol.* **1995**, *2*, 409−418.

(7) Nordlund, P.; Eklund, H. *J. Mol. Biol.* **1993**, *232*, 123−164.

(8) Stenkamp, R. E.; Jensen, L. H.; Sanders-Loehr, J. *Nature* **1981**, *291*, 263−264.

(9) (a) *Manganese Redox Enzymes;* Pecoraro, V. L., Ed.; VCH: New York, 1992. (b) Dismukes, G. C. *Chem. Rev.* **1996**, *96*, 2909−2926.

(10) (a) Kono, Y.; Fridovitch, I. J. *Biol. Chem.* **1983**, *258*, 6015. (b) Beyer, W. F., Jr.; Fridovitch, I. J. *Biochemistry* **1985**, *24*, 6460. (c) Khangulov, S. V.; Barynin, V. V.; Voevodskaya, N. V.; Grebenko, A. I. *Biochim. Biophys. Acta* **1990**, *1020*, 305.

(11) Barynin, V. V.; Vagin, A. A.; Melik-Adamyan, V. R.; Grebenko, A. I.; Khangulov, S. V.; Popov, A. N.; Andrianova, M. E.; Vainstein, A. *Dokl. Acad. Nauk. SSSR* **1986**, *288*, 877.

(12) (a) Follman, H.; Willing, A.; Auling, G.; Plonzig, J. In *Thioredoxin and Glutaredoxin Systems: Structure and Function;* Holmgren, A., Braeden, C. I., Joernvall, H., Sjöberg, B.-M., Eds.: Raven Press: New York, 1986; p 217. (b) Willing, A.; Follman, H.; Auling, G. *Eur. J. Biochem.* **1988**, *170*, 603.

S0020-1669(97)01537-1 CCC: $15.00
Published on Web 02/27/1998

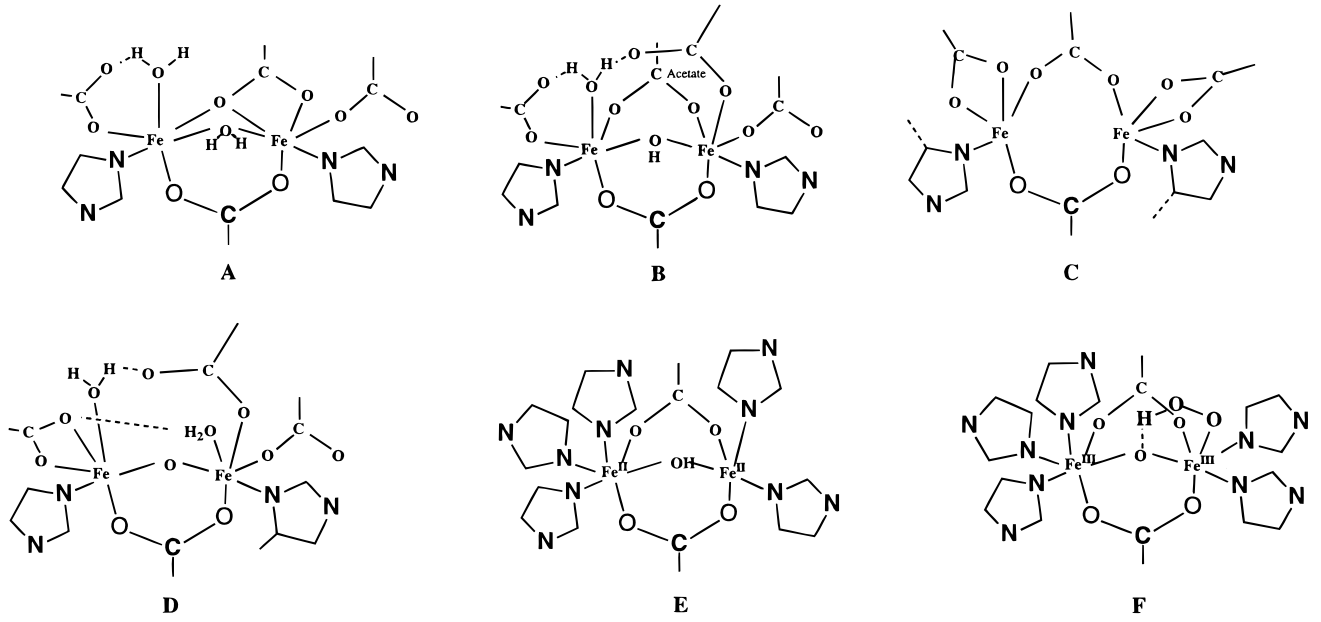

Figure 1. Carboxylate bridged dimers in (A) reduced MMO,[6] (B) oxidized MMO,[5] (C) reduced RRB2,[7] (D) oxidized RRB2,[7] (E) deoxyhemerythrin,[8] and (F) oxygenated hemerythrin.[8]

enzymes. Included among the trinuclear sites[13] are the tri-Zn centers in alkaline phosphatase,[14] P1-nuclease,[15] phospholipase,[16] and the tri-Mn center in inorganic pyrophosphatase.[17] Carboxylato-bridged dimanganese units may also exist in the tetramanganese photosynthetic oxidation center.[18]

The biological importance of bridged dinuclear iron structural units has stimulated extensive studies of model complexes. A large number of complexes that contain diiron μ-oxo or μ-hydroxo bridged by μ-*O*,*O*-carboxylate ligands have been reported and this chemistry has been critically evaluated in several excellent reviews.[19]

Among the dinuclear carboxylate complexes that have been synthesized and structurally characterized, an important subgroup consists of complexes with divalent metal ions. Of these the diferrous complexes often exhibit high reactivity toward O_2 or H_2O_2. Examples in this group include the $[M_2(\mu\text{-OAc})_2(OAc)_3(py)_2\mu\text{-}(OH_2)]^-$ anions[20] (M = Mn^{II}, Fe^{II} and Co^{II}), $[Fe_2(\mu\text{-OBz})(XDK)(ImH)_2(OBz)(MeOH)]$,[21] the $Fe_2(HPTB)(O_2CPh)_2$ complex that reacts irreversibly with O_2,[22] the $[Fe_2(H_2O)(O_2CR)_4(tmen)_2]$ complexes,[23] $[Fe_2(OAc)_2(TPA)_2]^{2+}$,[24] $[Fe(HB(3,5\text{-}^iPr2pz)_3]_2(OH)(OBz)$,[25] $[Fe_2(H_2hbab)_2(N\text{-}MeIm)_2]DMF$,[26] the $[Fe_2(O_2CH)_4(BIPhMe)_2]$ complex,[27] an asymmetric complex with both bridging and terminal formate ligands, and the $[(TACN)_2Fe(OH)(OAc)_2]^+$ complex.[28]

With very few exceptions the known diiron, di- or tri-bridged, synthetic analogue complexes are symmetric with the two iron subunits related by approximate (or crystallographically required) mirror planes or 2-fold axes. The terminal ligand coordination of the iron atoms for the majority of these complexes is effected by tridentate ligands such as 1,4,7-triazacyclononane (TACN),[28] (tris(1-pyrazolyl)hydroborate ($[HB(pz)_3]^-$),[25] or tris(2-pyridylmethyl)amine (tpa).[24] It would appear that these tridentate ligands impart thermodynamic stability to the dimers as a result of the chelate effect and may be important in determining the core structures. It should be emphasized, however, that dimeric, carboxylate-bridged, units are also obtained with simple monodentate or bidentate ligands.[20,23]

The coordination chemistry of oligomeric manganese complexes relevent to biological sites is also extensive.[29,30] Ex-

(13) Fenton, D. E.; Okawa, H. *J. Chem. Soc., Dalton Trans.* **1993**, 1350.
(14) Coleman, J. E. *Annu. Rev. Biophys. Biomol. Struct.* **1992**, *21*, 441.
(15) Volbeda, S.; Lahm, A.; Sakijama, F.; Suck, D. *EMBO J.* **1991**, *10*, 1607.
(16) Hough, E.; Hansen, L. K.; Birkness, B.; Junge, K.; Hansen, S.; Hordvik, A.; Little, C.; Dodson, E. J.; Derewenda, Z. *Nature* **1989**, *338*, 357.
(17) (a) Cooperman, B. S.; Baykov, A. A.; Lahti, R. *Trends Biochem. Sci.* **1992**, *17*, 262. (b) Chirgadze, N. Y.; Kuranova, I. P.; Veirskaya, N. A.; Teplyakov, A. V.; Wilson, K.; Srokopytov, B. V.; Harutynyan, E. G.; Hohne, W. *Kristallografiya* **1991**, *36*, 128.
(18) (a) Ghanotakis, D.; Yocum, C. F. *Annu. Rev. Plant Physiol. Mol. Biol.* **1990,** *41*, 255. (b) Pecoraro, V. L. *Photochem. Photobiol.* **1988**, *48*, 244. (c) Christou, G. *Acc. Chem. Res.* **1989**, *22*, 328.
(19) (a) Feig, A. L.; Lippard, S. J. *Chem. Rev.* **1994**, *94*, 759−805. (b) Kurtz, D. M. *Chem. Rev.* **1990**, *90*, 585−606. This review contains an extensive list of compounds reported prior to 1990. (c) Que, L., Jr.; Dong, Y. *Acc. Chem. Res.* **1996**, *29*, 190−196.
(20) Coucouvanis, D.; Reynolds, R. A., III.; Dunham, W. R. *J. Am. Chem. Soc.* **1995**, *117*, 7570−7571.
(21) (a) Herold, S.; Pence, L. E.; Lippard, S. J. *J. Am. Chem. Soc.* **1995**, *117*, 6134−6135. (b) Herold, S.; Lippard, S. J. *J. Am. Chem. Soc.* **1997**, *119*, 145−156. (c) OBz = the benzoate anion; ImH = imidazole; H2XDK = *m*-xylenediamine bis(Kemp's triacid) imide.
(22) (a) Dong, Y.; Menage, S.; Brennan, B. A.; Elgren, T. E.; Jang, H. G.; Pearce, L. L.; Que, L., Jr. *J. Am. Chem. Soc.* **1993**, *115*, *1851−1859.* HPTB= *N*,*N*,*N*′,*N*′-tetrakis(2-benzimidazolylmethyl)-2-hydroxy-1,3-diaminopropane, a dinucleating ligand.
(23) (a) Hagen, K. S.; Lachicotte, R. *J. Am. Chem. Soc.* **1992**, *114*, 8741−8742. (b) R = Me, Ph; tmen = *N*,*N*,*N*′,*N*′-tetramethyl-1,2-diaminoethane.
(24) (a) Ménage, S.; Zang, Y.; Hendrich, M. P.; Que, L., Jr. *J. Am. Chem. Soc.* **1992**, *114*, 7786−7792. (b) Oac = acetate, TPA = tris(2-pyridylmethyl)amine.
(25) (a) Kitajima, N.; Tamura, N.; Tanaka, M.; Moro-oka, Y. *Inorg. Chem.* **1992**, *31*, 3342−3343. (b) OBz = the benzoate anion; $HB(3,5\text{-}^iPr2pz)_3$ = tris (3,5-isopropylpyrazolyl) borate.
(26) (a) Stassinopoulos, A.; Schulte G.; Papaefthymiou, G. C.; Caradonna, J. P. *J. Am. Chem. Soc.* **1991**, *113*, *8686−8697.* (b) H2hbab = 1,2-bis(2-hydroxybenzamido)benzene; N-MeIm = *N*-methylimidazole.
(27) (a) Tolman, W. B.; Liu, S.; Bentsen, J. G.; Lippard, S. J. *J. Am. Chem. Soc.* **1991**, *113*, 152−164. (b) BIPhMe = 2,2′-bis(1-methyliimidazolyl)phenylmethoxymethane.
(28) (a) Hartman, J. R.; Rardin, R. L.; Chaundhuri, P.; Pohl, K.; Wieghardt, K.; Nuber, B.; Weiss, J.; Papaefthymiou, G. C.; Frankel, R. B.; Lippard, S. J. *J. Am. Chem. Soc.* **1987**, *109*, 7387−7396. (b) TACN = 1,4,7-trimethyl-1,4,7-triazacyclononane.
(29) Wieghardt, K. *Angew. Chem., Int. Ed. Engl.* **1989**, *28*, 1153−1172.

amples of synthetic dimeric Mn^{II} complexes include the symmetric $[Mn_2(O_2CC_2F_5)_4(H_2O)_3L_2]$[31] and the μ-aquabis(μ-carboxylato)$(L)_2Mn^{II}$ complexes.[32]

The possible lack of structural integrity in solution presents a problem regarding the identity of the reactive species when the kinetically labile "model" complexes (particularly the diiron species) participate in stoichiometric or catalytic substrate oxidation reactions involving O_2 or H_2O_2. Recently, various neutral iron carboxylate complexes[33] were found effective as catalysts in the oxidation of adamantane under conditions similar to those employed in the GiF system.[34] The latter is based on reactions of ferrous iron with dioxygen in a pyridine/acetic acid mixture that contains elemental zinc, and affords as products 2-adamantanone (major product) and 1- and 2-adamantanol (minor products).

Previously we communicated the synthesis and structural characterization of the Et_4N^+ salts of the X-ray isomorphous and isostructural $[M_2(OAc)_5(py)_2\mu\text{-}(OH_2)]^-$ complexes, **I** (M = Mn, Fe, Co).[20] In solution the complexes **I** are kinetically labile and exist in equilibria with other species that may be isolated when other counterions are present.[35] In this paper we report the detailed synthesis and charaterization of the $[M_2(OAc)_5(py)_2\mu\text{-}(OH_2)]Et_4N$ complexes, **I** (M = Mn, Fe, Co), and their rearrangement or dissociation into other products in acetonitrile solution. The reactions of the **I-Fe** complex with O_2, H_2O_2 and ferrocenium, and the catalytic oxidation of adamantane with **I-Fe** and its derivatives under GiF conditions also have been investigated.

Experimental Section

General Data. All reactions were carried out under an atmosphere of purified nitrogen using standard Schlenk techniques or in a Vacuum Atmospheres glovebox. The metal acetates, tetraethylammonium acetate tetrahydrate, and tetraethylammonium chloride were purchased from Aldrich and used as received. Ferrocenium hexafluorophosphate was synthesized by the sulfuric acid oxidation of ferrocene in the presence of hexafluorophosphate.[36] Pyridine was freshly distilled over calcium hydride and stored over 3 Å molecular sieves. Diethyl ether was predried over sodium wire and distilled from sodium benzophenone ketyl. Acetonitrile was predried over 3 Å molecular sieves and distilled over boric anhydride. Dichloromethane and propionitrile were distilled over calcium hydride. Electronic spectra were obtained on a Varian Cary model 219 spectrophotometer. Infrared spectra were obtained on a Nicolet 60-DX FT-IR spectrophotometer. Gas chromatography was performed on a Hewlett-Packard 5890 Series II instrument equipped with a flame ionization detector. Elemental analysis were performed by the Analytical Services of the University of Michigan.

Synthesis. (a) $[Mn_2(OAc)_5(py)_2\mu\text{-}(OH_2)]Et_4N$ (I-Mn). To a light pink solution of manganous acetate tetrahydrate (0.68 g, 2.78 mmol) in 25 mL of pyridine was added tetraethylammonium acetate tetrahydrate (0.365 g, 1.4 mmol). After stirring for 2 h the solution was filtered and 150 mL of diethyl ether was added to the filtrate to induce precipitation. A nearly colorless microcrystalline product was isolated (0.91 g, 1.28 mmol, 91% yield). Anal. Calcd for $Mn_2O_{11}N_3C_{36}H_{47}$ (fw 711.64): C, 47.35; H, 6.66; N, 5.92. Found: C, 46.79; H, 6.55; N, 5.63. Characteristic mid-IR bands (cm^{-1}): 2982 (m), 1620 (vs), 1577 (vs), 1567 (vs), 1446 (vs), 1416 (s), 1037 (m), 1009 (m), 795 (w), 705 (s), 656 (m), 615 (m). Far-IR (cm^{-1}): 419 (s br). Electronic spectra, nm (ϵ, M^{-1} cm^{-1}): featureless in pyridine and dichloromethane. Magnetic moment, μ_{eff}^{corr}: at 250 K, 7.67μ_B; at 4 K, 2.16μ_B.

(b) $[Fe_2(OAc)_5(py)_2\mu\text{-}(OH_2)]Et_4N$ (I-Fe). This compound was obtained in a manner analogous to that described for **I-Mn** with ferrous acetate in place of manganous acetate tetrahydrate. A golden brown microcrystalline product was isolated (0.87 g, 1.22 mmol, 87% yield). Anal. Calcd for $Fe_2O_{11}N_3C_{36}H_{47}$ (fw 713.46): C, 47.12; H, 6.59; N, 5.89. Found: C, 47.28; H, 6.44; N, 6.14. Mid-IR identical to **I-Mn**. Far-IR (cm^{-1}): 420 (s br). Electronic spectra, nm (ϵ, M^{-1} cm^{-1}): (a) featureless in dichloromethane; (b) 375 (4000) in pyridine. Magnetic moment, μ_{eff}^{corr}: at 250 K, 7.62μ_B; at 4 K, 4.37μ_B.

(c) $[Co_2(OAc)_5(py)_2\mu\text{-}(OH_2)]Et_4N$ (I-Co). This compound was obtained in a manner analogous to that described for **I-Mn** with cobalt acetate tetrahydrate in place of manganous acetate tetrahydrate. A violet microcrystalline product was isolated (0.85 g, 1.18 mmol, 85% yield). Anal. Calcd for $Co_2O_{11}N_3C_{36}H_{47}$, (fw 719.62): C, 46.73; H, 6.54; N, 5.84. Found: C, 46.41; H, 6.61; N, 5.72. Mid-IR identical to **I-Mn**. Far-IR (cm^{-1}): 428 (s br). Electronic spectra, nm (ϵ, M^{-1} cm^{-1}): (a) in dichloromethane, 567 (600), 533 sh; 586 sh; (b) in pyridine, 512 (400). Magnetic moment μ_{eff}^{corr}: at 250 K, 6.76μ_B; at 4 K, 4.72μ_B.

(d) $[Mn_3(OAc)_8](Et_4N)_2$ (II-Mn). Recrystallization of $Mn_2(OAc)_5(py)_2\mu\text{-}(OH_2)(ET_4N)$ (**I-Mn**), (0.5 g, 0.703 mmol) from an acetonitrile diethyl ether solution led to the isolation of a small amount of oil and a pink crystalline solid. The crystalline material (0.25 g, 0.28 mmol) was obtained in a 60% yield based on manganese. Anal. Calcd for $Mn_3O_{16}C_{32}H_{64}N_2$ (fw 897.68): C, 42.82; H, 7.19; N, 3.12. Found: C, 42.85; H, 7.43; N, 3.12. Characteristic mid-IR bands (cm^{-1}): 2982 (m), 1607 (vs), 1566 (vs), 1420 (vs), 1006 (m), 793 (w), 663 (m), 617 (m). Far-IR (cm^{-1}): 482 (m). Electronic spectra, nm (ϵ, M^{-1} cm^{-1}): featureless in acetonitrile. Magnetic moment μ_{eff}^{corr}: at 250 K, 9.82μ_B; at 4 K, 5.50μ_B.

(e) $[Fe_3(OAc)_8](Et_4N)_2$ (II-Fe). This compound was obtained in a manner analogous to that described for **II-Mn**. A small amount of oil and a colorless crystalline solid, which loses its crystallinity upon removal of the crystallization solvents, were isolated. The crystalline material (0.20 g, 0.22 mmol) was obtained in a 47% yield based on iron. Anal. Calcd for $Fe_3O_{16}C_{32}H_{64}N_2$, (fw 900.40): C, 42.69; H, 7.16; N, 3.11. Found: C, 42.14; H, 6.51; N, 2.96. Mid-IR identical to **II-Mn**. Far-IR (cm^{-1}): 472 (m). Electronic spectra, nm (ϵ, M^{-1} cm^{-1}): featureless in acetonitrile. Magnetic moment μ_{eff}^{corr}: at 250 K, 9.66μ_B; at 4 K, 5.57μ_B.

(f) $[Co_3(OAc)_8](Et_4N)_2$ (II-Co). This compound was obtained in a manner analogous to that described for **II-Mn**. A small amount of oil and a violet crystalline solid were isolated. The crystalline material (0.22 g, 0.24 mmol) was obtained in a 51% yield based on cobalt. Anal. Calcd for $Co_3O_{16}C_{32}H_{64}N_2$ (fw 909.66): C, 42.25; H, 7.09; N, 3.08. Found: C, 41.84; H, 6.77; N, 2.92. Mid-IR identical to **II-Mn**. Far-IR (cm^{-1}): 468 m (M−O). Electronic spectra, nm (ϵ, M^{-1} cm^{-1}): 607 sh, 575 (2900) and 539 sh in acetonitrile. Magnetic moment μ_{eff}^{corr}: at 250 K, 6.69μ_B; at 4 K, 4.39μ_B.

(g) $[Fe_3\mu_3\text{-}(O)(OAc)_7(OH_2)]Et_4N$ (III). An amount of $[Fe_2(OAc)_5(py)_2\mu\text{-}(OH_2)]Et_4N$ (**I-Fe**, 0.75 g, 1.05 mmol), was dissolved in 50 mL of propionitrile, exposed to the atmosphere for 30 min, and then filtered under a nitrogen atmosphere. An amount of diethyl ether (150 mL) was slowly deposited on top of the solution and allowed to diffuse slowly. Large brown block crystals formed and were isolated (0.32 g, 0.46 mmol, 65% yield) based on iron. Anal. Calcd for $Fe_3O_{16}C_{22}H_{43}N$ (fw 745.12): C, 35.46; H, 5.82; N, 1.88. Found: C, 35.80; H, 5.68; N, 1.93. Characteristic mid-IR bands (cm^{-1}): 3025 (w br), 2981 (m), 1622 (s), 1600 (vs), 1580 (s), 1421 (vs), 1004 (m), 802 (m), 660 (m), 619 (w). Electronic spectra, nm (ϵ, M^{-1} cm^{-1}): 463 (550) sh in acetonitrile. Magnetic moment μ_{eff}^{corr}: at 250 K, 5.62μ_B; at 4 K, 4.75μ_B.

(30) Pecoraro, V. L.; Baldwin, M. J.; Gelasco, A. *Chem. Rev.* **1994**, *94*, 807−826.
(31) Caneschi, A.; Ferraro, F.; Gatteschi, G.; Melandri, M. C.; Rey, P.; Sessoli, R. *Angew. Chem., Int. Ed. Engl.* **1989**, *28*, 1365−1366.
(32) (a) Yu, S.-B.; Lippard, S. J.; Sheweky, I.; Bino, A. *Inorg. Chem.* **1992**, *31*, 3502−3504. (b) L = Me_2bipy or tmeda.
(33) (a) Singh, B.; Long, J. R.; Papaefthymiou, G. C.; Stavropoulos, P. J. *J. Am. Chem. Soc.* **1996**, *118*, 5824−5826. (b) Singh, B.; Long, J. R.; Fabrizi de Biani, F.; Gatteschi, D.; Stavropoulos, P. J. *J. Am. Chem. Soc.* **1997**, *119*, 7030−7047.
(34) (a) Barton, D. H. R.; Doller, D. *Acc. Chem. Res.* **1992**, *25*, 504−512. (b) Barton, D. H. R.; Boivin, J.; Motherwell, W. B.; Ozbalik, N.; Schwartzentruber, K. M.; Jankowski, K. *New J. Chem.* **1986**, *10*, 387−398. (c) Barton, D. H. R.; Boivin, J.; Gastiger, M.; Morzycki, J.; Hay-Motherwell, R. S.; Motherwell, W. B.; Ozbalik, N.; Schwartzentruber, K. M. *J. Chem. Soc., Perkin Trans. 1* **1986**, 947−955.
(35) Reynolds, R. A., III; Pike, J. D.; Dunham, W. R.; Coucouvanis, D. Manuscript in preparation.
(36) Hadjikyriacou, A. Ph.D. Thesis, The University of Michigan, Ann Arbor, MI, 1988.

Table 1. X-ray Crystallographic and Data Collection Parameters for $[M_2(OAc)_5\mu\text{-}(H_2O)(py)_2]Et_4N$ (**I**) (M = Mn, Fe, Co); $[M_3(OAc)_8](Et_4N)_2$ (**II**) (M = Mn, Co); $[Fe_3(OAc)_7\mu_3\text{-}(O)(H_2O)]Et_4N$ (**III**); and $[Fe_4O_2(OAc)_6Cl_2(py)_4]$ (**IV**)

	I-Mn	I-Fe	I-Co	II-Mn	II-Co	III	IV
fw	711.64	713.46	719.62	897.67	909.64	744.6	996.96
space group	$P2_1/a$	$P2_1/a$	$P2_1/a$	$Aba2$	$P2_1nb$	$P42_11$	$Fdd2$
a (Å)	18.09(1)	18.085(6)	18.143(3)	18.794(4)	14.339(3)	19.496(7)	35.705(7)
b (Å)	11.057(4)	10.955(4)	10.888(2)	16.894(3)	16.719(3)	19.496(7)	12.762(3)
c (Å)	18.367(7)	18.273(7)	18.216(3)	14.165(3)	18.604(4)	8.716(4)	18.574(4)
α (deg)	90	90	90	90	90	90	90
β (deg)	108.49(4)	108.58(3)	108.84(1)	90	90	90	90
γ (deg)	90	90	90	90	90	90	90
V (Å^3)	3456(2)	3432(2)	3406(1)	4497(2)	4460(2)	3313(3)	8464(3)
Z	4	4	4	4	4	4	8
d_{calc} (g/cm^3)	1.35	1.38	1.40	1.33	1.36	1.49	1.57
d_{obs} (g/cm^3)	1.38	1.42	1.44	1.36	1.42	1.54	1.53
radiation	Mo Kα/graphite monochromator						
scan type	ω						
no. of data collcd	*a*	*a*	*a*	*b*	*b*	*b*	*b*
no. of unique reflcns	4541	4468	4459	3002	6012	3038	1032
ref $F\sigma^2 > 3\sigma(F\sigma^2)$	2099	2505	2578	1548[c]	3065[c]	2057	973[c]
no. of params	307	405	405	178	348	523	173
R_c	0.0592	0.0425	0.0473	0.0761	0.0793	0.0741	0.0440
R_w	0.0591	0.0431	0.0464	0.1066	0.1014	0.0744	0.0471
GOF	1.382	1.119	1.255	1.514	1.440	1.812	1.197

[a] $+h, +k, \pm l$, $2\theta = 3-45°$. [b] $+h, +k, +l$, $2\theta = 3-45°$. [c] $F\sigma^2 > 2\sigma(F\sigma^2)$.

(h) $Fe_4\mu_3\text{-}(O)_2(OAc)_6(py)_4Cl_2$ (IV). An amount of $[Fe_2(OAc)_5(py)_2\mu\text{-}(OH_2)]Et_4N$ (**I-Fe**, 1.00 g, 1.40 mmol), was dissolved in 40 mL of pyridine, and tetraethylammonium chloride (0.23 g, 1.40 mmol) was added to the solution. An excess of hydrogen peroxide (0.10 mL of 30 wt %) was added slowly to this solution. After stirring for 2 h the red-brown solution was filtered in air, and 50 mL of diethyl ether was added to the filtrate. Upon standing at −10 °C for 12 h, off-white crystalline tetraethylammonium acetate formed and was isolated. An additional 75 mL of diethyl ether was added to the deeply colored filtrate, which resulted in the formation of a red-brown crystalline material. The product was isolated and washed with a minimal amount of cold ethanol (0.51 g, 0.51 mmol, 36% yield). Anal. Calcd for $Fe_4O_{14}C_{32}H_{38}N_4Cl_2$ (fw 996.6): C, 38.53; H, 3.81; N, 5.62. Found: C, 39.04; H, 4.05; N, 5.77. Characteristic mid-IR bands (cm^{-1}): 1586 (s), 1445 (s), 1040 (w), 697 (m), 662 (w), 654 (w), 629 (w), 618 (w). Electronic spectra, nm (ϵ, M^{-1} cm^{-1}): 582 (270), 474 (1470) sh., 445 (2270) sh in acetonitrile. Magnetic moment μ_{eff}^{corr}: at 250 K, 4.49μ_B; at 4 K, 0.46μ_B.

(i) $[Fe_3\mu_3\text{-}(O)(OAc)_6(py)_3]$ (V). An amount of $[Fe_2(OAc)_5(py)_2\mu\text{-}(OH_2)]Et_4N$ (**I-Fe**, 0.75 g, 1.05 mmol) was dissolved in 50 mL of dichloromethane, and ferrocenium hexafluorophosphate (0.35 g, 1.05 mmol) and Et_3N were added. After standing for an hour, diethyl ether (100 mL) was slowly added on top of the solution. Large brown-black needles formed and were isolated (0.43 g, 55 mmol, 79% yield) based on iron. Anal. Calcd for $Fe_3O_{13}C_{27}H_{33}N_3$ (fw 775.11): C, 41.84; H, 4.29; N, 5.42. Found: C, 42.06; H, 4.44; N, 5.51. Characteristic mid-IR bands (cm^{-1}): 1611 (s), 1603 (s), 1447 (s), 1415 (s), 1041 (w), 699 (m), 656 (w), 632 (w). The compound is identical to the known basic acetate complex reported previously.[37]

Adamantane Oxidations.[34] Adamantane (0.1 g, 0.734 mmol) and an excess of zinc powder (1.3 g, 19.9 mmol) are dissolved/suspended in 29 mL of pyridine. To this was added 1 mL of a standard solution of the iron catalyst (10 mg/mL in pyridine) and complexes **I-Fe**, **II-Fe**, **III**, and **IV**, and the reaction was stirred vigorously in air for 18 h. Water was added (20 mL), and the mixture was extracted with diethyl ether (100 mL, three times). The ether solution was washed with 1 M HCl (100 mL, three times) followed by a saturated NaCl solution (100 mL, three times) and then dried over anhydrous $MgSO_4$. Following the evaporation of the solvent to dryness, the residue was dissolved in 10 mL of diethyl ether and an aliquot (5 mL) of this solution was combined with an aliquot (5 mL) of a standardized solution of naphthalene (10 mM in diethyl ether). This mixture was then analyzed by gas chromatography[38] for adamantane, naphthalene, 1-adamantanol, 2-adamantanol, and 2-adamatanone.

X-ray Crystallography. Single crystals of **I-Mn**, **I-Fe**, **I-Co**, and **IV** were grown by solvent diffusion of diethyl ether into mM solutions of the complexes in pyridine. Diffusion of diethyl ether into acetonitrile solutions of **II-Mn** and **II-Co**, and a propionitrile solution of **III** afforded single crystals for these complexes. The crystals were mounted in glass capillaries and sealed under argon. Diffraction data for all crystals were collected on a Nicolet R3m diffractometer using Mo Kα radiation equipped with a graphite monochromator. The solutions of the structures were determined by a combination of heavy-atom Patterson techniques, direct methods, and Fourier methods. The integrity of the crystals were monitored by following three standard reflections every ninety-seven reflections. Crystal and refinement data for complexes **I**−**IV** are compiled in Table 1.

(a) $[Mn_2(OAc)_5(py)_2\mu\text{-}(OH_2)]Et_4N$ (I-Mn). The carbon atoms of the tetraethylammonium cation and the carbon atoms of the pyridine ligands were refined using isotropic thermal parameters. The remaining non-hydrogen atoms were refined using anisotropic thermal parameters. The hydrogen atoms of the bridging water were not located in the electron density map.

(b) $[Fe_2(OAc)_5(py)_2\mu\text{-}(OH_2)]Et_4N$ (I-Fe). All non-hydrogen atoms were refined using anisotropic thermal parameters. The hydrogen atoms of the bridging water were located in the electron density map and were refined using isotropic thermal parameters.

(c) $[Co_2(OAc)_5(py)_2\mu\text{-}(OH_2)]Et_4N$ (I-Co). All non-hydrogen atoms were refined using anisotropic thermal parameters. The hydrogen atoms of the bridging water were located in the electron density map and were refined using isotropic thermal parameters.

(d) $[Mn_3(OAc)_8](Et_4N)_2$ (II-Mn). The carbon atoms were refined using isotropic thermal parameters. The remaining non-hydrogen atoms were refined using anisotropic thermal parameters.

(e) $[Co_3(OAc)_8](Et_4N)_2$ (II-Co). The carbon atoms of the tetraethylammonium cation were refined using isotropic thermal parameters. The remaining non-hydrogen atoms were refined using anisotropic thermal parameters.

(f) $[Fe_3\mu_3\text{-}(O)(OAc)_7(OH_2)]Et_4N$ (III). All non-hydrogen atoms were refined using anisotropic thermal parameters.

(37) Cannon, R. D.; White, R. P. *Prog. Inorg. Chem.* **1988**, *36*, 195−298.

(38) The products were analyzed by a flame ionization detector. Column: 3% OV-17; column held at 90 °C for 2 min and then ramped to 160 °C at 10 °C/min; injector and detector set at 250 °C; flow rate 200 mL/min. Retention time (min): 6.3, adamantane; 9.4, naphthalene; 11.0, 1-adamantanol; 12.2, 2-adamantanol; and 13.4, 2-adamatanone.

(g) $Fe_4\mu_3$-$(O)_2(OAc)_6(py)_4Cl_2$ (IV). The carbon atoms were refined using isotropic thermal parameters. The remaining non-hydrogen atoms were refined using anisotropic thermal parameters.

Results and Discussion

Synthesis. The previously communicated[20] dinuclear complexes $[M_2(OAc)_5(py)_2\mu$-$(OH_2)]^-$ (M = Mn, Fe, Co) assemble spontaneously from the appropriate reagents in pyridine solution and are isolated as Et_4N^+ salts, **I**−**M**. The metal ions are asymmetrically bridged by two acetate ligands and a water molecule. One of the metal ions is bound by a pyridine ligand and two monodentate acetate ligands, that are hydrogen bonded to the bridging water molecule. The second metal ion is bound to a bidentate acetate ligand and a pyridine ligand. In the absence of pyridine and upon dissolving these compounds in acetonitrile changes in the electronic spectra are apparent for **I-Fe** and **I-Co**. These changes suggest that upon dissociation of pyridine the kinetically labile complexes rearrange to form new molecules. The spectra observed in pyridine solutions of **I-Fe** and **I-Co** can be "recovered" upon addition of small amounts of pyridine to the acetonitrile solutions of these complexes.

Recrystallization of **I** from neat acetonitrile affords a small amount of an oily residue and the linear trinuclear complexes $M_3(OAc)_8(Et_4N)_2$ (**II-M**, M = Mn, Fe, Co). The electronic spectra of $[M_3(OAc)_8](Et_4N)_2$ (M = Fe (**II-Fe**), Co (**II-Co**)) in acetonitrile solutions are similar to those seen for $[M_2(OAc)_5$-$(py)_2\mu$-$(OH_2)]Et_4N$ (M = Fe (**I-Fe**), Co (**I-Co**)) respectively, in acetonitrile solutions. The electronic spectra **II-Fe** and **II-Co** taken in pyridine solutions or acetonitrile solutions with pyridine added (5% v/v) are similar to those of **I-Fe** and **I-Co**, respectively, in pyridine solutions. Subsequent recrystallization of **II-Fe** and **II-Co** from wet pyridine leads to the reformation of the dinuclear species **I-Fe** and **I-Co** which can be isolated. This observation is consistent with an equilibrium between **I** and **II** (eq 1), although a number of other ionic and neutral

$$2[M_2(OAc)_5(py)_2\mu\text{-}(OH_2)]^- \rightleftharpoons [M_3(OAc)_8]^{2-} + M(OAc)_2 + 4py + 2H_2O \quad (1)$$

species may also be present. In contrast to the iron and cobalt complexes recrystallization of **II-Mn** from wet pyridine affords the trinuclear species unchanged, suggesting that **II-Mn** may be thermodynamically more stable than **I-Mn**.

Manganese(II) complexes are known to be oxidized to Mn(III) and Mn(IV) complexes, often with terminal and/or bridging O^{2-} ligands, by oxygen and peroxides.[29,30] The reaction of the dinuclear **I-Mn** with oxygen (air) or hydrogen peroxide in acetonitrile solution affords a small amount of a dark brown oil and the $[M_3(OAc)_8]^{2-}$ complex **II-Mn** in a 65% yield. In pyridine solution again a small amount of a dark brown oil is isolated along with the unreacted starting material **I-Mn**, recovered in a 85% yield. Presumably the dark brown material contains oxidized manganese species. These materials were not characterized due to their poor yields and difficulty in their separation from **I-Mn** and **II-Mn**.

Air oxidation of **I-Fe** in propionitrile affords the mixed-valence trinuclear complex $[Fe_3\mu_3$-$(O)(OAc)_7(OH_2)]Et_4N$ (**III**). The $[Fe_3\mu_3$-$(O)(OAc)_5]^+$ core of **III** is quite similar to the $[Fe_3\mu_3$-$(O)(OAc)_6]^{0,1+}$ cores of the basic acetate complexes[37] (vide infra).

The hydrogen peroxide or air oxidation of **I-Fe** in pyridine in the presence of tetraethylammonium chloride was investigated with the expectation that the presence of additional counterions

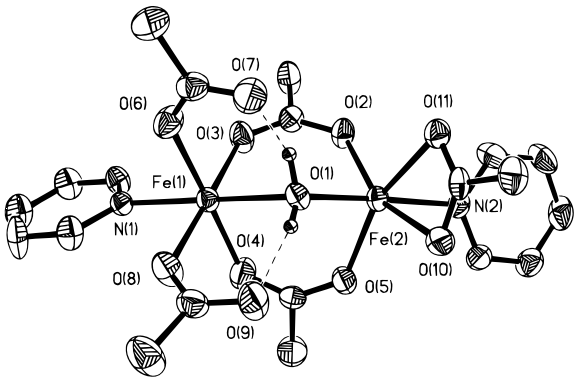

Figure 2. Structure and partial labeling of the anion $[Fe_2(OAc)_5(Py)_2\mu$-$(OH_2)^-$, **I-Fe**, non-hydrogen atoms as drawn by ORTEP. Thermal ellipsoids represent the 40% probability surfaces except the water protons which were fixed for clarity.

(Et_4N^+ or Cl^-) or ligands (Cl^-) may facilitate the isolation of oxidation products. The tetranuclear complex $Fe_4\mu_3$-$(O)_2$-$(OAc)_6(py)_4Cl_2$ (**IV**) was isolated and shows a rhombic $\{Fe^{III}_4$-$(\mu_3-O)_2\}$ "butterfly" core previously seen in iron and manganese chemistry.[18c,39] Attempts to assemble this compound from $FeCl_2$, $Fe(OAc)_2$ (3 equiv) in pyridine or pyridine/CH_3CN solution in the presence of O_2, H_2O_2, or O_2/H_2O_2 were not successful. These results support the hypothesis that the integrity of **I-Fe** is maintained to some extent in pyridine solution, as well as in equilibria with other species, and is in concert with the synthetic methodology used by others to make tetranuclear iron complexes with similar structural motifs.[39,40]

In an attempt to isolate a hydroxide bridged mixed-valence complex of **I-Fe** by oxidation and the subsequent monodeprotonation of the bridging water molecule, an equivalent amount of ferrocenium ion in the presence of an equimolar amount of base was added to a solution of **I-Fe**. The compound isolated was the well-studied, mixed-valence $Fe_3(OAc)_6\mu_3$-$(O)(py)_3$ complex[37] (**V**), with the basic acetate structure.

Structure Descriptions. The complexes $[M_2(OAc)_5(Py)_2\mu$-$(OH_2)]Et_4N$, **I** (M = Mn, Fe, Co; Figure 2), are X-ray isomorphous and isostructural. Selected bond distances and angles are compiled in Table 2. The anions of **I** consist of two six-coordinate divalent metal ions bridged by two acetate ligands and one water ligand. The asymmetry in the dimeric structures derived from the differences in the coordination environment of the two metal ions. One of these is coordinated by two monodentate anionic acetate ligands and a pyridine molecule, while the other is bound to a bidentate acetate ligand and a pyridine molecule. The two monodentate acetate ligands bound to the same metal ion are hydrogen bonded to the aqua bridge in the dimers. This results in a uniquely asymmetric bridge, by comparison to other aqua-bridged dimers that are hydrogen bonded in a symmetric fashion by monodentate carboxylate ligands located symmetrically on either side of the bridge.[23,34,41] In **I** the O(ac)−$O(H_2)$ distances of 2.547(1) and 2.60(1) Å for **I-Mn**, 2.574(7) and 2.615(8) Å for **I-Fe**, and 2.573(8) and 2.612(9) Å for **I-Co** are within range for strong hydrogen bonding. The Mn−Mn distance in **I-Mn** of 3.618(3) Å compares well to the distances reported for $[Mn_2(O_2CC_2F_5)_4$-$(H_2O)_3L_2]$[31] and the aqua-bridged complexes $Mn_2\mu$-$(OH_2)\mu_2$-

(39) Armstrong, W. H.; Roth, M. E.; Lippard, S. J. *J. Am. Chem. Soc.* **1987**, *109*, 6318−6326.
(40) Gorun, S. M.; Lippard, S. J. *Inorg. Chem.* **1988**, *27*, 149−156.
(41) (a) Ahlgrén, M.; Turpeinen, U. *Acta Crystallogr.* **1982**, *B38*, 276. (b) Turpeinen, U.; Hämäläinen, R.; Reedijk, J. *Polyhedron* **1987**, *6*, 1603. (c) Das, B. K.; Chakravarty, A. R. *Inorg. Chem.* **1991**, *30*, 4978.

Table 2. Interatomic Distances (Å) and Angles (deg) for $[M_2(OAc)_5\mu\text{-}(H_2O)(py)_2]Et_4N$ **(I)** (M = Mn, Fe, Co); $[M_3(OAc)_8](Et_4N)_2$ **(II)** (M = Mn, Co); and $[Fe_3(OAc)_7\mu_3\text{-}(O)(H_2O)]Et_4N$ **(III)**[a]

	Distances (Å)					
complex	M−M[b]	M−O	M−O(μ-OAc)	M−O(η^1-OAc)[c]	M−O(η^2-OAc)[d]	M−N
I− Mn	3.618(3)	2.252(7)	2.14(2, 4)	2.141(8)	2.259(7)	2.290(9)
		2.111(6)		2.167(7)	2.262(8)	2.314(8)
I-Fe	3.577(2)	2.206(6)	2.09(2, 4)	2.110(5)	2.195(6)	2.210(6)
		2.148(5)		2.098(5)	2.228(4)	2.222(6)
I-Co	3.548(2)	2.146(6)	2.06(1, 4)	2.084(5)	2.183(5)	2.167(6)
		2.111(5)		2.068(6)	2.181(6)	2.173(6)
II-Mn[e]	3.569(2)	2.11(2)	2.12(7, 4)[f]	2.143(13)	2.195(10)	−
		2.17(2)			2.282(9)	
II-Co	3.465(3)	2.222(12)	2.06(2, 8)[g]	2.298(14)	2.20(4, 5)[h]	−
	3.471(3)	2.106(13)		2.190(13)		
		2.138(11)				
		2.072(11)				
III	3.283(3)	1.867(4)	2.06(8, 4)[i]	2.040(9)	2.231(9)	2.120(10)[j]
	3.283(3)	1.867(4)			2.120(8)	
	3.344(3)	2.093(10)				

	Angles (deg)					
	I-Mn	**I-Fe**	**I-Co**	**II-Mn**	**II-Co**	**III**
M-(μ-O)-M[k]	108.3(3)	110.5(2)	112.9(2)	113.1(8)	106.6(5)	111.8(3)
					110.8(5)	111.8(3)
						127.1(4)

[a] The first number in parentheses represents the largest of the individual standard deviations or the standard deviation of the mean, and the second represents the number of equivalent bonds averaged out. [b] **I**, μ-H_2O; **II**, μ-O of η^1,μ^2 acetate ligand; **III**, μ_3−O. [c] **I**, monodentate acetate; **II**, η^1-O of η^1,μ^2 acetate ligand; **III**, singular bridging acetate. [d] **I**, **II**, and **III** bidentate acetate. [e] Disorder of η^1,μ^2 acetate ligand and μ acetate modeled at 50% occupancy. [f] Range 2.09(2)−2.195(10). [g] 1.990(10)−2.108(12). [h] 2.189(10)−2.306(12). [i] 1.983(8)−2.142(9). [j] M−OH_2. [k] **I**, M−μ-H_2O−M; **II**, M−μ-O−M of η^1,μ^2 acetate ligand; **III**, two Fe^{II}−μ_3-O−Fe^{III} and Fe^{III}−μ_3-O−Fe^{III}.

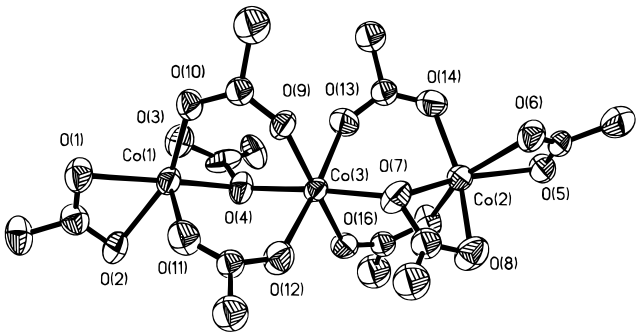

Figure 3. Structure and partial labeling of the anion $[Co_3(OAc)_8]^{2-}$, **II-Co**, non-hydrogen atoms as drawn by ORTEP. Thermal ellipsoids represent the 30% probability surfaces.

$(O_2C\ R)_2L_2$[32] of 3.739(2), 3.595(9), and 3.621(2) Å, respectively. The Fe−Fe distance in **I-Fe** of 3.577(2) Å compares well to the distances reported for $Fe_2\mu$-$(OH_2)(O_2CR)_4(tmen)_2$ (3.653(2) Å),[23] deoxyhemerythrin (3.57 Å),[42] and methane monooxygenase (3.5 Å).[6] The Co−Co distance in **I-Co** of 3.548(2) Å is comparable to the distances in $Co_2\mu$-$(OH_2)(O_2C\ R)_4(tmen)_2$[41b] complexes of 3.597 and 3.696 Å. Other metric details (Table 2) are similar to those reported for a plethora of carboxylate complexes and will not be discussed further.

The centrosymmetric anions of $[M_3(OAc)_8](Et_4N)_2$, **II** (Figure 3), consist of a linear array of three six-coordinate divalent metals. They contain six acetate ligands that are found in three different coordination modes. Two of the acetate ligands are bound as bidentate chelates, one each to the two terminal metal ions. Two acetate ligands in the μ_1,μ_2 mode and one acetate ligand in the μ_1,η_1 mode are bridging the central metal ion to each of the terminal metal ions. The $M_3(OAc)_6$ core is similar to that found in $Mn_3(O_2CR)_6(bipy)_2$[18c,43] and $Mn_3(O_2CCH_3)_6$-$(biphme)_2$[44] as well as in $Co_3(O_2CR)_6(B)_2$[45] (B = monodentate base). A series of complexes of the general type $Fe_3(O_2CR)_6$-$(L)_2$ (L = ^{i}PrOX, PheMe$_3$Eda)[46] have been shown to have the same core as in **II-Mn** and **II-Co**. However, when a more sterically hindered chelate is used (L = BIPhOH, BIDPhEH) the μ_1,η_1 acetate no longer binds to the terminal iron ion and the geometry of the terminal iron ions becomes distorted square pyramidal. The central manganese ion in **II-Mn** is located on a crystallographic 2-fold axis and exhibits a disorder associated with the 2-fold axis. This disorder can be modeled (Figure 4) with a 50% occupancy for each of the two different bridging modes (μ_1,μ_2 and μ_1,η_1). The two remaining μ_1,μ_2 bridging acetate ligands are unperturbed. The Mn−Mn distance in **II-Mn** at 3.569(2) Å is comparable to distances found in $Mn_3(O_2CCH_3)_6(biphme)_2$,[44] $Mn_3(O_2CCH_3)_6(phen)_2$,[44] $Mn_3(O_2CPh)_6(bipy)_2$,[18c] and $Mn_3(O_2CCH_3)_6(bipy)_2$[43] at 3.635(1), 3.700(2), 3.387(1), 3.588(1), and 3.614(1) Å, respectively. The **II-Co** complex does not have any imposed crystallographic symmetry and does not display disorder in the bridging acetate ligands. The Co−Co distances in **II-Co** at 3.465(3) and 3.471(3) Å are comparable to that in $Co_3(O_2CPh)_6(quinoline)_2$[45a] at 3.56 Å.

The anion of $[Fe_3\mu_3\text{-}(O)(OAc)_7(OH_2)]Et_4N$, **III** (Figure 5), consists of three iron atoms bound to a central μ_3-O. The iron centers form an isosceles triangle with two Fe−Fe distances of 3.283(3) and one of 3.344(3) Å with the μ_3-O displaced above the trigonal plane of the irons by 0.34 Å. A crystallographic mirror plane bisects the molecule through the μ_3-O and the

(42) Zhang, K.; Stern, E. A.; Ellis, F.; Sanders-Loehr, J.; Schiemke, A. K. *Biochemistry* **1988**, *27*, 7470−7479.

(43) Ménage, S.; Vitols, S. E.; Bergerat, P.; Codjovi, E.; Kahn, O.; Girerd, J.-J.; Guillot, M.; Solans, X.; Calvet, T. *Inorg. Chem.* **1991**, *30*, 2666−2671.

(44) Rardin, R. L.; Poganiuch, P.; Bino, A.; Goldberg, D. P.; Tolman, W. B.; Liu, S.; Lippard, S. J. *J. Am. Chem. Soc.* **1992**, *114*, 5240−5249.

(45) (a) Catterick, J.; Hursthouse, M. B.; New, D. B.; Thornton, P. *J. Chem. Soc., Chem. Commun.* **1974**, 843−844. (b) Catterick, J.; Thornton, P. *J. Chem. Soc., Dalton Trans.* **1976**, 1634.

(46) Goldberg, D. P.; Telser, J.; Bastos, C. M.; Lippard, S. J. *Inorg. Chem.* **1995**, *34*, 3011−3024.

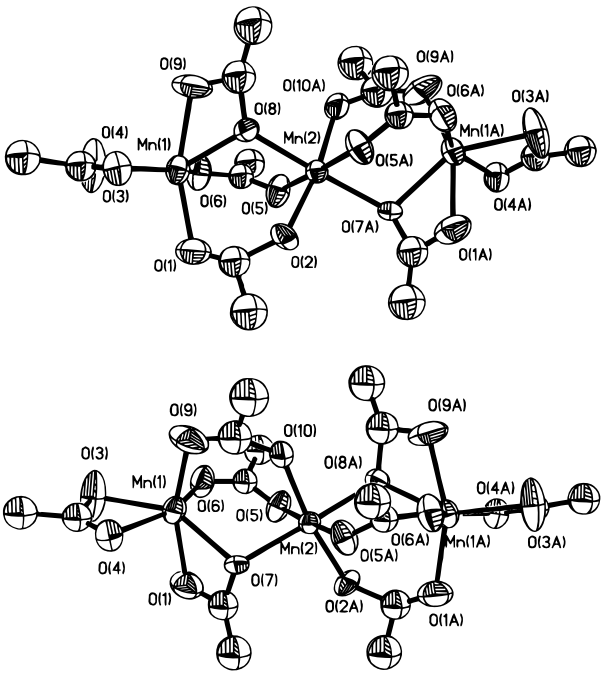

Figure 4. Structure and partial labeling of the anion $[Mn_3(OAc)_8]^{2-}$, **II-Mn**, non-hydrogen atoms as drawn by ORTEP. Thermal ellipsoids represent the 30% probability surfaces. Shown are two forms that occupy the same site in the positionally disordered structure; the disordered oxygen atoms O2, O7, O8, and O10 were refined at 50% occupancy.

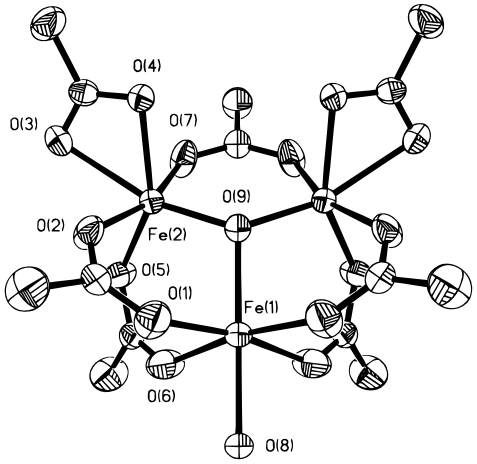

Figure 5. Structure and partial labeling of the anion $[Fe_3\mu_3\text{-}(O)(OAc)_7(OH_2)]^-$, **III**, non-hydrogen atoms as drawn by ORTEP. Thermal ellipsoids represent the 40% probability surfaces.

unique iron. The remaining iron atoms are in equivalent environments and are each bound to a terminal bidentate acetate. A single acetate bridges the two equivalent iron atoms in the familiar μ_1,μ_2 bridging mode. Two additional μ_1,μ_2 bridging acetate ligands connect each of the equivalent iron atoms to the unique iron atom. All of the iron centers are in a distorted octahedral environment, with a terminal water ligand completing the coordination sphere of the unique iron. The asymmetric $(Fe_3O)^{6+}$ core of **III** is similar to the core in the well-studied basic acetate complexes.[37] Valence localization in the mixed-valence basic acetate complexes usually arises from intermolecular and crystal lattice effects caused by solvent molecules at low temperatures which destroy the 3-fold symmetry of the molecule.[37,47] The asymmetry in **III**, by comparison to the triiron basic acetate structures, is due to the absence of one μ_1,μ_2 bridging acetate. In the absence of a full complement of

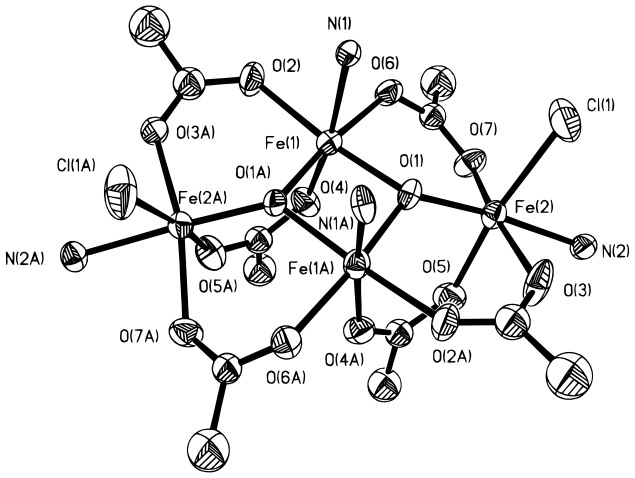

Figure 6. Structure and partial labeling of $Fe_4\mu_3\text{-}(O)_2(OAc)_6(py)_4Cl_2$, **IV**, non-hydrogen atoms as drawn by ORTEP; carbon atoms of the pyridine ligands were omitted for clarity. Thermal ellipsoids represent the 40% probability surfaces.

bridging acetate ligands the iron atoms are found in two different coordination environments that appear to structurally promote valence localization to two ferric sites and one ferrous site. The Fe−(μ_3-O) bond distances in **III**, two at 1.867(4) and one at 2.093(10) Å, are comparable to those found in $Fe_3(OAc)_6\mu_3\text{-}(O)(3\text{-Et-py})_3\cdot 0.5(\text{toluene})$[47] at 1.866(4), 1.858(4), and 2.006(4) Å. The latter contains a lattice-stabilized valence-localized $[Fe^{II}Fe^{III}{}_2\mu_3\text{-}(O)]$ core. The valence localization in **III** is apparent in the ^{57}Fe Mössbauer spectra (vide infra).

The structure of $Fe_4\mu_3\text{-}(O)_2(OAc)_6(py)_4Cl_2$, **IV** (Figure 6), shows the rhombic M_4O_2 core previously encountered in manganese[18c] and iron[39,40,48]chemistry. The $(Fe_4O_2)^{8+}$ unit in **IV** is similar to those in $[Fe_4\mu_3\text{-}(O)_2(O_2CPh)_7(H_2B(pz)_2)_2](Et_4N)$,[39] **VI**; $Fe_4\mu_3\text{-}(O)_2(O_2CCF_3)_8(H_2O)_6\cdot 2H_2O$,[48] **VII**, as well as $[Fe_4\mu_3\text{-}(O)_2(BiCOH)_2(BiCO)_2(O_2CPh)_4]Cl_2$.[47] A structural comparison of the cores in **IV, VI,** and **VII** is presented in Table 3. The $(Fe_4O_2)^{8+}$ unit in **IV** displays crystallographically imposed C_2 symmetry with bond angles and distances which correspond well to those in **VI** which has approximate C_2 symmetry. In contrast to the "butterfly" core of **IV** and **VI**, **VII** has planar D_{2h} symmetry. The gross structures of **IV** and **VI** are very similar, with each of the external irons of **IV** bound to terminal chloride and pyridine ligands in place of the binucleating $H_2B(pz)_2$ ligands in **VI**. In **IV** two terminal pyridine ligands have taken the place of the unique bridging benzoate ligand in **VI**. These pyridine ligands are found in a syn conformation that may be stabilized by $\pi-\pi$ interactions. The displacement of the external iron atoms in **IV** from the mean plane of the Fe_2O_2 inner core (0.6 Å), is smaller than that in **VI** (0.9 Å). This difference accounts for a less puckered structure for the core in **IV** and longer Fe_1-Fe_1 and Fe_2-Fe_2 distances compared to **VI**.

Magnetic Susceptibility. The temperature-dependent magnetic behavior for the $[M_2(OAc)_5(Py)_2\mu\text{-}(OH_2)]Et_4N$ (**I**) complexes was analyzed, and coupling constants (Table 4) were derived from fits obtained using the spin Hamiltonian,[49] $\mathbf{H} = -2J\mathbf{S}_1\cdot\mathbf{S}_2$. In fitting the susceptibility the high-temperature

(47) Wu, C.-C.; Jang, H. G.; Rheingold, A. L.; Gütlich, P.; Hendrickson, D. N. *Inorg. Chem.* **1996**, *35*, 4137−4147.
(48) (a) Ponomarev, V. I.; Atovmyan, L. O.; Bobkova, S. A.; Turté, K. I. *Dokl. Acad. Nauk. SSSR* **1984,** *274*, 368−372. (b) Stucken, R. A.; Ponomarev, V. I.; Nifontov, V. P.; Turté, K. I.; Atovmyan, L. O. *J. Struct. Chem.* **1985**, *26*, 197−201.
(49) Griffith, J. S. *Struct. Bonding* **1972**, *10*, 87−126.

Table 3. Interatomic Distances (Å) and Angles (deg) for $Fe_4(\mu_3\text{-}O)_2(OAc)_6(py)_4Cl_2$ (**IV**); $[Fe_4(\mu_3\text{-}O)_2(OAc)_7(H_2B(pz_2)_2]Et_4N$ (**VI**);[a] and $Fe_4(\mu_3\text{-}O)_2(OCCF_3)_8(H_2O)_6\ 2H_2O$ (**VII**)[b]

	IV	**VI**	**VII**
	Distances (Å)		
Fe_1-Fe_1	2.878(3)	2.829(4)	2.915(3)
Fe_1-Fe_2	3.462(2)	3.488(2)	3.476(2)
	3.316(2)	3.500(2)	3.436(3)
		3.326(2)	
		3.330(2)	
Fe_2-Fe_2	6.032(3)	5.920(2)	6.276(4)
Fe_1-O	1.907(7)	1.895(7)	1.936(3)
	1.945(7)	1.917(7)	1.961(3)
		1.955(8)	
		1.967(8)	
Fe_2-O	1.861(7)	1.822(7)	1.842(4)
		1.854(8)	
	Angles (deg)		
Fe_1-O-Fe_1	96.7(3)	93.5(3)	96.5(2)
		94.5(3)	
Fe_1-O-Fe_2	123.2(4)	125.1(5)	129.5(2)
	130.9(4)	125.9(5)	133.9(2)
		133.6(5)	
		134.1(5)	
$O-Fe_1-O$	83.1(3)	85.4(3)	82.9(2)
		85.6(3)	

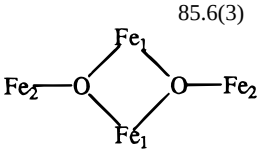

[a] Reference 39. [b] Reference 48.

Table 4. Summary of Magnetic Suceptibilities for Complexes **I**−**IV**

	μ_{eff}		J (cm^{-1})	
Complex	at 250 K	at 4 K	J_{12}	J_{13}
I-Mn	7.67	2.16	−1.0	−
I-Fe	7.62	4.37	−0.2	−
I-Co	6.76	4.72	−0.2	−
II-Mn[a]	9.83	5.52	−5.6	0.7
II-Fe	9.66	5.57	−1.4	0
II-Co	6.69	4.39	−7.0	0
III	5.62	4.75	−	−
IV	4.49	0.46	−	−

[a] $Fe_1-Fe_2-Fe_3$, $J_{12} = J_{23}$.

asymptote was used to determine the g values for each of the component moments in the dimers: $g = 2.0$ for **I-Mn**, $g = 2.2$ for **I-Fe**, and $g = 2.19$ for **I-Co**, which are close to the expected values.[50] Magnetization studies do not show zero-field effects, and since the coupling was very weak and because they would not contribute significantly to the understanding of the behavior of these complexes, the zero-field splitting terms were ignored in the calculation. The very weak anti-ferromagnetic coupling for these complexes (M = Mn, Fe, Co) are as expected for aqua-bridged dinuclear complexes and in line with the anti-ferromagnetic coupling strength order $O^{2-} > OH^- > H_2O$ usually observed for similarly bridged species. The magnetic moments for $Mn_2\mu\text{-}(OH_2)(O_2CC(CH_3)_3)_2bipy_2$ and $Mn_2\mu\text{-}(OH_2)(OAc)_4(tmeda)_2$[32] of 7.769$\mu_B$ at 300 K, 0.914μ_B at 2 K, 8.02 μ_B at 300 K, and 0.671μ_B at 2 K, respectively, are similar to the values for **I-Mn**, as are their weak anti-ferromagnetic coupling constants of −2.7 and −2.9 cm^{-1}. Coupling constants of aqua-bridged iron species have been reported to be typical of anti-ferromagnetic behavior and are significantly weaker then those obtained for OH^--bridged species.[23] Weak anti-ferromagnetic coupling has also been recently observed for a series of diferrous XDK complexes with bridging benzoate, trifluorosulfonate, and chloride ligands.[21b]

The temperature-dependent magnetic behavior for the $[M_3(OAc)_8](Et_4N)_2$ (**II**) complexes was analyzed, and coupling constants were derived (Table 4) from fits obtained using the spin Hamiltonian,[49,51] $\mathbf{H} = -2J_{12}(\mathbf{S_1 \cdot S_2}) + -2J_{13}(\mathbf{S' \cdot S_3})$ assuming that $J_{12} = J_{23}$, due to the symmetry of the complexes, and $\mathbf{S'} = \mathbf{S_1} + \mathbf{S_2}$. With $\mathbf{S} = \mathbf{S_1} + \mathbf{S_2} + \mathbf{S_3}$, $\mathbf{H} = J_{12}(|\mathbf{S_1}|^2 + |\mathbf{S_2}|^2 - |\mathbf{S'}|^2) + J_{13}(|\mathbf{S'}|^2 + |\mathbf{S_3}|^2 - |\mathbf{S}|^2)$. If zero-field terms are ignored, the magnetic susceptibilty can be calculated (eq 2).[52]

$$x = (L\,\beta^2 g^2/3kT)[(\sum S(S+1)(2S+1)e^{-E(\mathbf{S},\mathbf{S'})/kT})/(\sum(2S+1)e^{-E(\mathbf{S},\mathbf{S'})/kT})] \quad (2)$$

where $(L\,\beta^2/3k) = 0.5013$ erg K mol^{-1}. The derived coupling constants $J_{12} = J_{23}$ and J_{13} show weak anti-ferromagnetic behavior for **II-Mn** and compare well to those for the structurally similar $Mn_3(O_2CCH_3)_6(bipy)_2$[43] complex. The latter has a magnetic moment of 9.75μ_B at 285 K and 5.88μ_B at 4.2 K and $J_{12} = -4.4$ cm^{-1} and $J_{13} = \pm 0.5$ cm^{-1}. Another complex with the same core, $Mn_3(O_2CCH_3)_6(biphme)_2$,[44] also has similar magnetic properties with a magnetic moment of 9.85μ_B at 300 K and 5.54μ_B at 2 K and $J_{12} = -1.9$ cm^{-1} and $J_{13} = -0.3$ cm^{-1}.

Recently a magnetic study of a series of complexes, $Fe_3(O_2CR)_6(L)_2$ (L = ^{i}PrOX, PheMe$_3$Eda, BIPhOH, BIDPhEH),[46] which possess the same $[Fe_3(O_2CR)_6]$ core as in **II**, were shown to exhibit both ferromagnetic and anti-ferromagnetic coupling. The complexes $Fe_3(O_2CPh)_6(^iPrOX)_2$ and $Fe_3(O_2CPh)_6(PheMe_3Eda)_2$ displayed weak anti-ferromagnetic behavior. The magnetic moments of 9.52μ_B at 300 K and 6.52μ_B at 5 K and $J_{12} = -1 \pm 0.5$ cm^{-1} and $J_{13} = 0$ cm^{-1} for the ^{i}PrOX and 9.50μ_B at 300 K and 6.74μ_B at 5 K and $J_{12} = -1 \pm 0.5$ cm^{-1} and $J_{13} = 0$ cm^{-1} for the PheMe$_3$Eda derivative compare well to the values determined for **II-Fe**. The derivatives with L = BIPhOH or BIDPhEH were weakly ferromagnetic. The later ligands are bound to $[Fe_3(O_2CR)_6]$ cores that have four μ_1,μ_2 bridging carboxylate ligands and the remaining carboxylate ligands bridge through a single oxygen with the second oxygen "dangling". The difference between the ^{i}PrOX and PheMe$_3$Eda and the BIPhOH and BIDPhEH derivatives undoubtedly has its origin in the steric constraints associated with the bulky BIPhOH and BIDPhEH ligands. These constraints cause the terminal iron atoms to assume a trigonal bipyramidal rather than octahedral geometry. In the absence of structural characterization of **II-Fe**, its speculative structure can only be derived from other physical measurements. Its anti-ferromagnetic behavior, similar to that for $Fe_3(O_2CPh)_6(^iPrOX)_2$ and $Fe_3(O_2CPh)_6(PheMe_3Eda)_2$ where the terminal iron atoms are six-coordinate, supports the assumption that **II-Fe** is isostructural to **II-Mn** and **II-Co**. The terminal iron atoms in **II-Fe** would not be five-coordinate as found with the BIPhOH or BIDPhEH ligands but rather six-coordinate as found with the ^{i}PrOX or PheMe$_3$Eda terminal ligands as in **II-Mn** and **II-Co**.

The magnetic moment of $[Fe_3\mu_3\text{-}(O)(OAc)_7(OH_2)]Et_4N$, **III**, 5.62$\mu_B$ at 250 K, is significantly larger than for the mixed-valence basic acetate complexes, ∼3.1μ_B at 280 K.[37] The

(50) Drago, R. S. *Physical Methods in Chemistry*; Saunders College Publishing: Chicago, 1977.
(51) Kambe, K. *J. Phys. Soc. Jpn.* **1950**, *5*, 48.
(52) Van Vleck, J. H. In *The Theory of Electric and Magnetic Susceptibilities*; Oxford University Press: London, 1932.

observed moment for **III** indicates weaker anti-ferromagnetic coupling in **III** by comparison to the basic acetate complexes, where the coupling constants range from 35−50 cm^{-1} to 10−20 cm^{-1} with a variety of terminal ligands and lattice solvent molecules.[37] This may be the result of valence localization in **III**, apparent in the Mössbauer spectrum and the structural analysis, which shows a longer $Fe^{II}-\mu_3$-(O) bond distance which may decrease the effectiveness of the magnetic exchange between the iron atoms.

The magnetic moments of $Fe_4\mu_3$-$(O)_2(OAc)_6(py)_4Cl_2$, **IV**, 4.49μ_B at 250 K (2.25μ_B per iron atom) and 0.46μ_B at 4 K (0.23μ_B per iron atom), are indicative of moderate anti-ferromagnetic coupling. The magnetic behavior of **IV** is consistent with that of the structurally similar complex **VI**.[39] An analysis of the variable temperature magnetic susceptibility data for **III** and **IV** using spin-exchange coupling models is currently underway.

Mössbauer Spectroscopy. The solid-state Mössbauer spectrum of **I-Fe** at 125 K displays only a single sharp quadrupole doublet with δ(Fe) = 1.30(1) mm/s, ΔE_q = 2.00 mm/s, and fwhm = 0.15 mm/s.[53] In frozen pyridine solution **I-Fe** also displays a single sharp quadrupole doublet with δ(Fe) = 1.18(1) mm/s, ΔE_q = 2.96 mm/s, and fwhm = 0.20 mm/s indicating that the solid-state structure of **I-Fe** is not retained in pyridine solution. The isomer shifts and quadrupole splittings in the solid state and frozen pyridine solution, however, are typical for high-spin ferrous complexes. The observance of only a single quadrupole doublet for the asymmetric complex was unexpected but not unique and reflects similar electric field gradients for the two iron sites in both the solid state and frozen pyridine solution. A single quadrupole doublet for asymmetric iron sites has also been reported for $[Fe_2(O_2CCH_3)_4(py)_3]_n$.[33] The Mössbauer spectra of **I-Fe** in the solid state and in frozen pyridine solution reflect the kinetic lability of **I**, which in solution undergoes a structural rearrangement. This lability also is demonstrated by its rearrangement upon recrystallization from acetonitrile and by differences in the solution electronic spectra obtained in pyridine and acetonitrile solutions. The isomer shift of **I-Fe** in the solid state is comparable to values reported for $Fe_2\mu$-$(OH_2)(O_2CR)_4(tmen)_2$,[23] MMO_{red},[54] and $RRB2_{red}$[1d,f] as well as the series of XDK complexes.[21b] The ΔE_q value is smaller for **I-Fe** presumably due to a lesser distortion of the iron sites in **I-Fe** from octahedral symmetry compared to those in other diiron complexes.

The solid-state Mössbauer spectrum of $[Fe_3(OAc)_8](Et_4N)_2$ (**II-Fe**) at 125 K displays two quadrupole doublets with δ(Fe) = 1.22(1), 1.14(1) mm/s and ΔE_q = 1.71, 2.50 mm/s with a relative intensity of 2:1. These values are typical for high-spin ferrous ions and are similar to that seen in $[Fe_3(O_2CPh)_6$-$(BIPhMe)_2]$[44] which shows two quadrupole doublets with δ-(Fe) = 1.14(1), 1.36(1) mm/s; and ΔE_q = 3.60, 2.64 mm/s with a relative intensity of 2:1. The lesser isomer shift in the terminal iron ions in $[Fe_3(O_2CPh)_6(BIPhMe)_2]$ in comparison to the central metal ion and the terminal ions in **II-Fe** arises from the presence of the π acceptor aromatic nitrogen atoms of the BIPhMe ligands.

The solid-state Mössbauer spectrum of **III** (Figure 7) at 125 K displays two quadrupole doublets with δ(Fe) = 1.29(1) and 0.48 mm/s, ΔE_q = 1.89 and 0.71 mm/s, and relative intensities of 1:2, respectively. The isomer shift values of **III** agree well with those reported for the mixed-valence $Fe_3(OAc)_6$ μ_3-(O)-(3-Et-py)$_3$·0.5(toluene)[47] complex of 1.242 and 0.531 mm/s with respect to iron at 99 K. The quadrupole splittings are different as would be expected due to differences in the overall charges that will affect the electric field gradient.

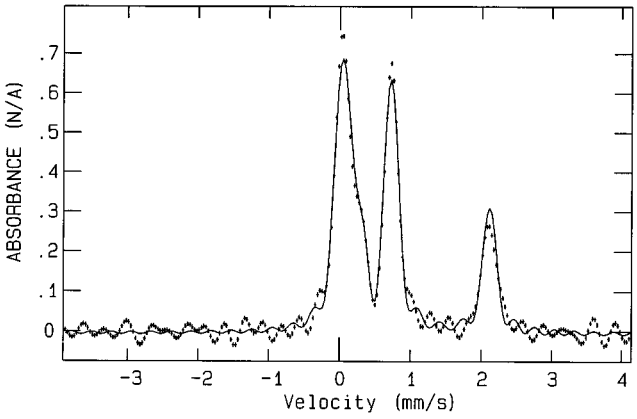

Figure 7. Solid state Mössbauer spectrum of **III** at 125 K.

The solid-state Mössbauer spectrum of **IV** at 125 K displays only a single quadrupole doublet with δ(Fe) = 0.492 mm/s and ΔE_q = 0.848 mm/s. A similar result was reported for the tetranuclear **VI** which shows a single quadrupole doublet with δ(Fe) = 0.52 mm/s and ΔE_q = 1.21 mm/s at 80 K.[39] The difference in the ΔE_q values reflects a more symmetric electric field gradient in **IV**. An examination of the structure of **IV** with comparison to **VI** (Table 3) shows that the departure of the iron sites in **IV** from octahedral symmetry is less pronounced than that observed for the iron sites in **VI**. Thus the $Fe-\mu_3$-(O) bond distances in **IV** range from 1.861(7) to 1.945(7) Å, while those in **VI** are found between 1.842(4) and 1.961(3) Å. The spectrum of **VII** displays[48] two resolvable quadrupole doublets at 80 K. The Mössbauer spectrum of the structurally similar complex $[Fe_4\mu_3$-$(O)_2(BiCOH)_2(BiCO)_2(O_2CPh)_4]Cl_2$[40] at 4.2 K is nearly identical to **IV** with one quadrupole doublet (δ(Fe) = 0.5 mm/s and ΔE_q = 0.81 mm/s).

Adamantane Oxidation. The oxidations of adamantane with **I-Fe**, **II-Fe**, **III**, and **IV** as catalysts were investigated. The conditions and protocol of the catalytic oxidation were those described for the GiF system.[34] In a pyridine/acetic acid solution the substrate is dissolved along with an iron catalyst and a sacrificial reducing agent (Zn metal). After vigorous stirring in the air for 18 h, the solution is analyzed for oxidation (and coupling) products. The products observed are 1-adamantanol, 2-adamantanol, 2-adamantanone, 4-(1-adamantyl)pyridine, and 2-(1-adamantyl)pyridine, the pyridine-substituted adamantyl products were not investigated in this preliminary study. The results obtained when **I-Fe**, **II-Fe**, **III**, and **IV** were used as catalysts and a comparison to the data obtained from the GiF system[34] and for certain neutral iron acetate[33] complexes are shown in Table 5.

The results show the catalytic effectiveness of all of these compounds to be very similar. The percentages of total oxidized products for **I-Fe**, **II-Fe**, **III**, and **IV** are very similar to those reported previously,[33,34] with **I-Fe** being the most effective of the catalysts reported herein. The **I-Fe** and **II-Fe** catalysts show oxidation selectivity that favors the formation of 1-adamantanol over 2-adamantanol. This is in contrast to what has been seen previously in the other systems[33,34] where 2-adamantanol is the preferred product. The catalytic studies reported herein were undertaken with the sole purpose of demonstrating that under GiF conditions a great number of complexes that contain the proper chemical constituents display similar catalytic function.

(53) "fwhm", full width half-maximum.

(54) Liu, K. E.; Valentine, A. M.; Wang, D.; Huynh, B. H.; Edmondson, D. E.; Salifoglou, A.; Lippard, S. J. *J. Am. Chem. Soc.* **1995**, *117*, 10174−10185.

Table 5. Catalytic Oxidation of Adamantane by O_2 by Various Iron Carboxylate Complexes[a]

catalyst	1-ad-ol[b]	2-ad-ol[c]	2-ad-one[d]	total	ref
I	1.9[e]	0.8	10.0	12.7	this work
I[f]	3.2	1.2	12.5	16.9	this work
II	2.0	0.5	7.5	10.0	this work
III	0.9	0.9	8.5	10.3	this work
IV	1.0	0.8	8.1	9.9	this work
S1[g]	0.5	1.4	11.7	13.6	33
S2[h]	0.6	1.3	11.3	13.2	33
S3[i]	0.7	1.3	10.1	12.1	33
B[j]	1.4	1.9	12.2	15.5	34

[a] Carried out under GiF conditions.[34] [b] 1-Adamantanol. [c] 2-Adamantanol. [d] 2-Adamantanone. [e] Percent of product relative to initial concentration of adamantane. [f] Carried out under 1 atm of pure O_2. [g] $Zn_2Fe(OAc)_6(py)_2$. [h] $Fe(OAc)_2(py)_4$. [i] $[Fe_2(OAc)_4(py)_3]_n$. [j] GiF system.

The mechanistic details of the GiF system have been studied extensively and some disagreement regarding the interpretations of the data can be found in the literature.[55] The lability of iron acetate complexes in solution, as shown by the chemistry of **I-Fe** and **II-Fe**, as well as the presence of essentially the same chemical components in all of the catalytic systems examined thus far, suggests that the active catalyst(s) in the above systems may be a common complex(es) of considerable thermodynamic stability. However to make assumptions about the nature of the active GiF catalyst based on the complexes isolated from these catalytic reactions or from catalytic studies of kinetically labile "models" is not prudent. The solid state structures of the complexes that are used as catalysts may have no relation to the species performing catalysis. A number of potential catalytic species may be present in solution in equilibria. Some of these may be isolated under specific conditions, and any or all of them could function as catalysts or precatalysts under the conditions of the GiF system. We expect to gain some insight into the species that are possibly present in solution by identifying the species present in nonpolar solvent solutions prior to and following the catalytic oxidation. Studies with derivatives of **I-Fe** and **II-Fe**, soluble in nonpolar solvents, are currently in progress with the results to be communicated at a later date.

Summary and Conclusions

The synthesis and structural characterization of a series of divalent dinuclear asymmetrically bridged aqua complexes have been presented. The kinetic lability of these molecules in solution results in a structural diversity which becomes apparent by the choice of solvent and/or the counterions present.[35] The presence of simple, easy to replace ligands and the known stoichiometry of the isolated complexes make them well suited as starting materials for the synthesis of complexes that contain multidentate, structure-stabilizing, ligands.

The oxidation of **I-Fe** has led to the isolation of complexes **III** and **V**, which exhibit the $\{Fe_3\mu_3\text{-}(O)\}^{6+}$ core common in iron chemistry. Complex **IV** was also isolated as an oxidation product and exhibits a rhombic $\{Fe_4(\mu_3\text{-}(O))_2\}^{8+}$ unit also known in iron chemistry but to a much lesser extent than the $\{Fe_3\mu_3\text{-}(O)\}$ core.

Complexes **I-Fe**, **II-Fe**, **III**, and **IV** catalytically oxidize adamantane under GiF conditions. Due to the kinetic lability of these complexes in coordinating solvents, the exact nature of the catalyst(s) is difficult to ascertain. Comparison of the results obtained in this study with results from other laboratories on related complexes[33,34] shows remarkable similarities. It appears that in the absence of kinetic constraints many of these catalytic oxidations may be based on a common catalyst that assembles in solution from the common components that are present in all systems.

The structural similarity of **I-Fe** to the reduced form of MMO is apparent in the solid state. However, solutions of **I-Fe** in donor solvents do not retain the solid-state structure, and as a result a study of the oxidative function of **I-Fe**, and possibly the development of a functional model for MMO, is hindered. The inherent kinetic lability of iron−carboxylate complexes is general, with most of the known carboxylate complexes subject to structural rearrangement in solution. It is clear that carboxylate-bridged centers in metalloenzymes and metalloproteins retain their structural integrity by virtue of the protein "backbone" which serves as a matrix for the orientation of substrate molecules and the introduction of dioxygen to the active metal centers. An elementary study of enzyme function with "model" compounds lies in the development of synthetic analogue systems, for which solution kinetic lability is hindered and structural integrity is maintained.

Acknowledgment. This work was made possible by funding from the National Institutes of Health (GM-33080). The authors thank Mr. J. D. Pike for assistance with the catalytic oxidations of adamantane as well as Dr. Namdoo Moon and Mr. Thomas Butler for the Mössbauer Spectroscopy.

Supporting Information Available: Tables S1−S4 containing listings of positional parameters, thermal parameters and selected bond distances and angles of **II** (M = Mn, Co), **III**, and **IV** (33 pages). Ordering information is given on any current masthead.

IC971537P

(55) (a) Perkins, M. J. *Chem. Soc. Rev.* **1996,** 229−236. (b) Barton, D. H. R. *Chem. Soc. Rev.* **1996,** 237−239.